HEALTH AND MEDICINE

Exercise mimetics and JAK inhibition attenuate IFN-γ–induced wasting in engineered human skeletal muscle

Zhaowei Chen, Binjie Li, Ren-Zhi Zhan, Lingjun Rao, Nenad Bursac*

Chronic inflammatory diseases often lead to muscle wasting and contractile deficit. While exercise can have anti-inflammatory effects, the underlying mechanisms remain unclear. Here, we used an in vitro tissue-engineered model of human skeletal muscle ("myobundle") to study effects of exercise-mimetic electrical stimulation (E-stim) on interferon-γ (IFN-γ)–induced muscle weakness. Chronic IFN-γ treatment of myobundles derived from multiple donors induced myofiber atrophy and contractile loss. E-stim altered the myobundle secretome, induced myofiber hypertrophy, and attenuated the IFN-γ–induced myobundle wasting and weakness, in part by down-regulating JAK (Janus kinase)/STAT1 (signal transducer and activator of transcription 1) signaling pathway amplified by IFN-γ. JAK/STAT inhibitors fully prevented IFN-γ–induced myopathy, confirming the critical roles of STAT1 activation in proinflammatory action of IFN-γ. Our results reveal a previously unknown mechanism of the cell-autonomous anti-inflammatory effects of muscle exercise and establish the utility of human myobundle platform for studies of inflammatory muscle disease and therapy.

INTRODUCTION

Skeletal muscle comprises 45% of the total human body mass, and its contractile function is fundamental for the maintenance of life. Healthy skeletal muscle has a robust capacity to regenerate in response to minor injuries via activation, proliferation, and differentiation of muscle stem cells, a process that is greatly aided with the local and systemic inflammatory response (*1*). Interferon-γ (IFN-γ), in particular, is an important proinflammatory cytokine that regulates myogenic process during muscle regeneration, and its production is well balanced among natural killer (NK) cells, $CD4^+$ and $CD8^+$ T cells, and regulatory T cells (*2*). While inflammation following muscle injury promotes muscle regeneration, unregulated inflammatory reactions in many diseases, including chronic obstructive pulmonary disease, rheumatoid arthritis, dermatomyositis, cachexia, or sarcopenia, are associated with muscle loss and weakness (*3*–*6*). For example, sarcopenia is an age-associated syndrome characterized by progressive and generalized loss of skeletal muscle function and is usually associated with elevated expression of cytokines, including IFN-γ (*6*). In addition, elevated IFN-γ levels are routinely observed after influenza virus infection (*7*) and are associated with a cytokine storm resulting in tissue and organ damage in COVID-19 (*8*).

Besides numerous studies in rodents that show myopathic effects of inflammation in general and IFN-γ in particular (*9*–*14*), clinical studies have suggested that elevated IFN-γ in chronic inflammation and autoimmune diseases is one of major contributors to human skeletal muscle wasting and dysfunction (*5*, *6*, *15*). In a handful of in vitro studies in human muscle cells, IFN-γ has been shown to increase expression of human leukocyte antigen–DR isotype (HLA-DR) class II antigens (*16*), proteases cathepsin B and L (*17*), and cytokines CXCL9, CXCL10, interleukin-6 (IL-6), and transforming growth factor–β (TGF-β) (*18*, *19*), as well as to inhibit myoblast growth and fusion (*20*). On the other hand, specific functional consequences and underlying mechanisms of IFN-γ elevation in human skeletal muscle have not been previously studied in vitro due to shortcomings of two-dimensional (2D) muscle cell culture (*21*). Recently, we have reported the first generation of 3D tissue-engineered models of functional human skeletal muscle ("myobundles") made using primary myoblasts or induced pluripotent stem cell–derived myogenic progenitors (*22*–*24*). In optimized culture conditions, 3D human myobundles show superior myotube differentiation than 2D cultures and recapitulate the hallmark functional properties of native skeletal muscle including electrically or chemically induced twitch and tetanic contractions, a positive force-frequency relationship, robust calcium transients, and physiological responses to a diverse set of chemicals and drugs.

In more recent studies, we have shown that myobundles exhibit physiological response to exercise-mimetic electrical stimulation (E-stim) as evidenced from increased contractile strength, bulk muscle size, myotube diameter and length, sarcomeric protein expression, and glycolytic and fatty acid metabolism (*24*). In humans, E-stim and physical exercise can increase muscle mass and strength (*25*) and provide therapeutic benefits in the setting of chronic inflammation and aging (*26*–*28*). The anti-inflammatory effects of muscle exercise are usually attributed to paracrine action of working myofibers on nonmuscle cells including adipocytes, macrophages, T cells, and NK cells (*29*). On the other hand, whether exercised myofibers can exert cell-autonomous anti-inflammatory effects on muscle structure and function has not been previously studied.

Here, we used the human myobundle system devoid of complex organ-organ interactions present in vivo to first time explore direct effects of IFN-γ on human skeletal muscle structure, function, and cytokine secretion and to unveil potential muscle-autonomous mechanisms underlying anti-inflammatory roles of exercise. We found that IFN-γ treatment induced muscle atrophy and reduced contractile function in human myobundles via up-regulation of the JAK/STAT (Janus kinase/signal transducer and activator of transcription) pathway (*30*), an effect that was directly countered by exercise-mimetic muscle stimulation. We further showed that the block of JAK/STAT up-regulation by IFN-γ with small-molecule JAK inhibitors tofacitinib (*31*) and baricitinib (*32*), clinically used

Department of Biomedical Engineering, Duke University, Durham, NC, USA.
*Corresponding author. Email: nenad.bursac@duke.edu

for rheumatoid arthritis and in trials for COVID-19 (*33*), fully prevented muscle wasting and weakness induced by IFN-γ. Our findings establish human myobundles as a novel in vitro platform for studies of inflammatory muscle disease.

RESULTS

Exercise-mimetic E-stim counteracts IFN-γ–induced functional deficit in myobundles

On the basis of previous studies in mice (*9*), we set to explore whether chronic 7-day application of a proinflammatory cytokine IFN-γ (20 ng/ml) to human myobundles cultured in serum-free media would lead to induction of muscle atrophy and weakness. Human myobundles made using cells derived from three independent donors were differentiated for 1 week, then exposed to IFN-γ for 1 week, and assessed for changes in cytokine secretion, structural, biochemical, and functional properties (Fig. 1A). To assess whether exercise-mimetic activity of myobundles can reduce expected myopathic effects of IFN-γ, we simultaneously applied chronic intermittent E-stim regime shown to increase myobundle mass and strength in our previous study (Fig. 1B) (*24*). In isometric force tests, we found that compared with the untreated control, IFN-γ treatment reduced myobundle twitch and tetanic force amplitude by 66 and 68%, respectively (Fig. 1, C, D, and G), while applying E-stim to untreated myobundles doubled their strength (Fig. 1, C, E, and G). E-stim cotreatment with IFN-γ significantly increased myobundle contractile force compared with IFN-γ–only application (Fig. 1, D, F, and G), with twitch and tetanus amplitudes approximating those of untreated myobundles exposed to E-stim (Fig. 1, C, F, and G). These functional results were highly reproducible for myobundles from all three donors (fig. S1, A to C), as was the lack of any effects of IFN-γ or E-stim on passive tension measured at different stretch levels (fig. S1, D to F). Furthermore, measurements of force kinetics revealed that IFN-γ slowed both contraction (Fig. 1H) and relaxation (Fig. 1I) of myobundles and that E-stim rescued the IFN-γ–induced force relaxation deficit as evidenced from the return of twitch recovery time (RT1/2) to control value (Fig. 1I). The exact numerical results of functional measurements are presented in table S1. Together, these studies showed that IFN-γ exerts adverse, inflammatory effects on contractile function of human myobundles and that exercise-mimetic activity can prevent IFN-γ–induced muscle weakness.

E-stim prevents IFN-γ–induced structural deterioration of myobundles

We next investigated mechanisms underlying IFN-γ–induced myobundle weakness and functional benefit of E-stim, including possible changes in muscle structure, cytokine secretion, and calcium handling. From cross-sectional stainings (Fig. 2, A to C, and fig. S2, A to C), we found that both IFN-γ and E-stim similarly increased myobundle cross-sectional area (CSA) by ~40%, while E-stim of IFN-γ–treated myobundles did not induce additional CSA increase (Fig. 2D). Similar to our previous study (*24*), the number of nuclei

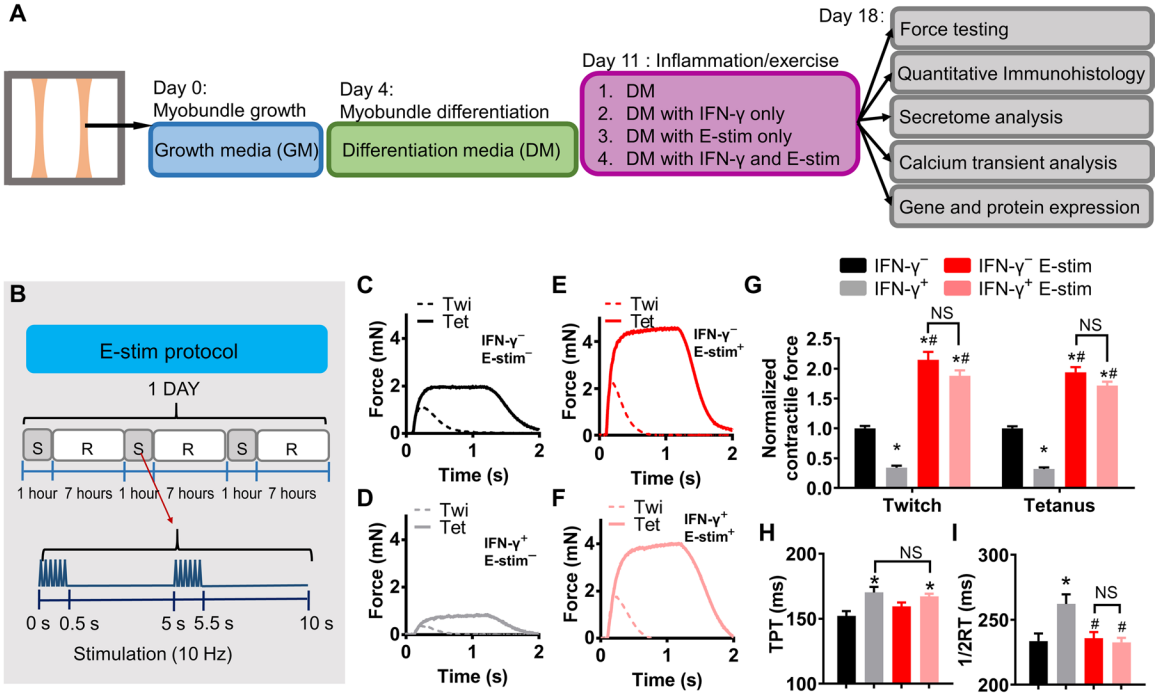

Fig. 1. Exercise-mimetic electrical stimulation (E-stim) counteracts IFN-γ–induced deficit in myobundle contractile function. (**A**) Schematic overview of myobundle culture, treatment, and characterization. Human primary myoblasts were expanded in 2D culture and mixed with hydrogel to form 3D myobundles, which were cultured in growth media (GM) for 4 days, then in differentiation media (DM) for 7 days, after which E-stim and/or IFN-γ (20 ng/ml) was applied for an additional 7 days. (**B**) E-stim protocol consisted of alternating 1-hour stimulation (S) at 10 Hz and 7-hour rest (R). (**C** to **F**) Representative twitch (Twi, 1 Hz) and tetanus (Tet, 20 Hz) force traces from myobundles (C) without IFN-γ or E-stim (IFN-γ^-, E-$stim^-$), (D) IFN-γ^+, E-$stim^-$, (E) IFN-γ^-, E-$stim^+$, and (F) IFN-γ^+, E-$stim^+$. (**G**) Twitch and tetanic force amplitudes averaged over three independent donors and shown relative to the IFN-γ^-, E-$stim^-$ group (n = 5 to 10 myobundles per donor, 20 to 23 myobundles per group). (**H** and **I**) Time-to-peak tension (H; TPT) and half-relaxation time (I; 1/2RT) derived from contractile force recordings in myobundles (n = 47 to 75 data points from 20 to 23 myobundles from three donors per group). *P < 0.05 versus IFN-γ^-, #P < 0.05 versus IFN-γ^+. NS, nonsignificant. Data are presented as means ± SEM.

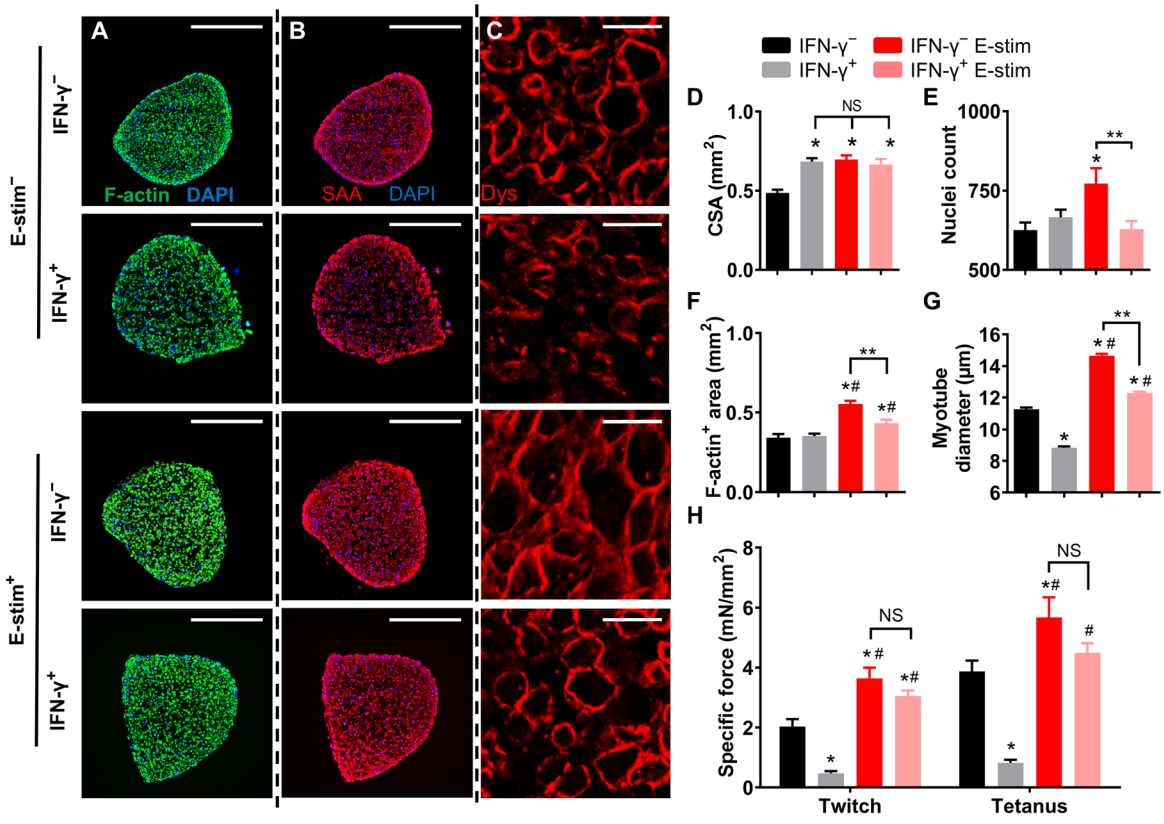

Fig. 2. E-stim prevents IFN-γ–induced structural deterioration of myobundles. E-Stim prevents IFN-γ–induced structural deterioration of myobundles. (**A** to **C**) Representative myobundle cross sections immunostained for (A) F-actin (green; scale bars, 500 μm), (B) sarcomeric α-actinin (SAA; red; scale bars, 500 μm), and (C) dystrophin (Dys; red; scale bars, 25 μm). (**D** to **G**) Quantification of (D) myobundle cross-sectional area (CSA), (E) number of nuclei per cross section, (F) F-actin$^+$ area, and (G) myotube diameter [n = 19 to 27 images from three donors per group, 3 to 5 myobundles for each donor for (D) to (F), n > 900 myotubes from three donors per group for (G)]. (**H**) Force amplitude normalized per myobundle CSA (specific force, n = 20 to 23 myobundles from three donors per group). *P < 0.05 versus IFN-γ$^-$, $^{\#}P$ < 0.05 versus IFN-γ$^+$, **P < 0.05. NS, nonsignificant. Data are presented as means ± SEM.

in myobundle cross section was significantly increased by E-stim in the absence of IFN-γ (Fig. 2E), while application of IFN-γ, with or without E-stim, resulted in unchanged nuclear numbers. Total F-actin$^+$ area, a measure of myobundle muscle mass, was not altered by IFN-γ, indicating that IFN-γ–induced force deficit was not a result of total muscle mass loss (Fig. 2F). On the other hand, E-stim induced muscle mass increase, albeit more in untreated (F-actin$^+$ area, 0.56 mm^2) than in IFN-γ–treated (0.43 mm^2) myobundles (Fig. 2F). We then assessed possible alterations in the myotube size by staining myobundle cross sections for dystrophin, a myotube membrane protein (Fig. 2C and fig. S2C). The IFN-γ treatment significantly reduced myotube diameter (11.3-μm untreated versus 8.8-μm IFN-γ treated) and area (fig. S2D), thus inducing myotube atrophy, whereas E-stim induced myotube hypertrophy by increasing myotube diameter and area in untreated and, to less extent, IFN-γ–treated myobundles (Fig. 2G and fig. S2D). We further examined density of myotubes [labeled by F-actin and sarcomeric α-actinin (SAA)] in myobundle cross sections and found that IFN-γ decreased myotube density, which remained at control levels in the presence of E-stim (fig. S2, E and F). Numerical results are presented in table S1. Together, these analyses suggest that IFN-γ–induced myotube size and density decrease were prevented in exercise-mimetic E-stim conditions. We also assessed specific force of myobundles (contractile force normalized by muscle CSA), and similar to effects on myotube size and density, we found that E-stim prevented IFN-γ–induced force decrease (Fig. 2H).

E-stim prevents IFN-γ–induced decrease of myotube length, sarcomere abundance, and contractile protein expression

We also cryosectioned myobundles longitudinally and immunostained them for F-actin and SAA to assess potential changes in myotube and sarcomere organization across the entire myobundle depth (Fig. 3, A and B, and figs. S3 and S4). Adverse effects of IFN-γ treatment were most apparent in the interior of myobundles as evident from the decrease in projected myotube length (L; Fig. 3C and fig. S3, A and B), alignment (movie S1), and sarcomeric organization with significantly reduced percentage of cross-striated myotubes (from 45% in IFN-γ$^-$ to 15% in IFN-γ$^+$ group; Fig. 3D and fig. S3, C to F). As in our previous study (*24*), E-stim significantly increased myotube length (Fig. 3C) and percentage of cross-striated myofibers in untreated and, to a less extent, in IFN-γ–treated myobundles (Fig. 3D), preventing the deteriorating effects of IFN-γ on myobundle structure. We then assessed changes in expression of contractile proteins (Fig. 3E) in myobundles and found that dystrophin and SAA expression remained unaltered with IFN-γ and E-stim treatments (Fig. 3, E to G), while changes in total myosin light chain (MYL) and myosin heavy chain (MYH) expression followed the same trend

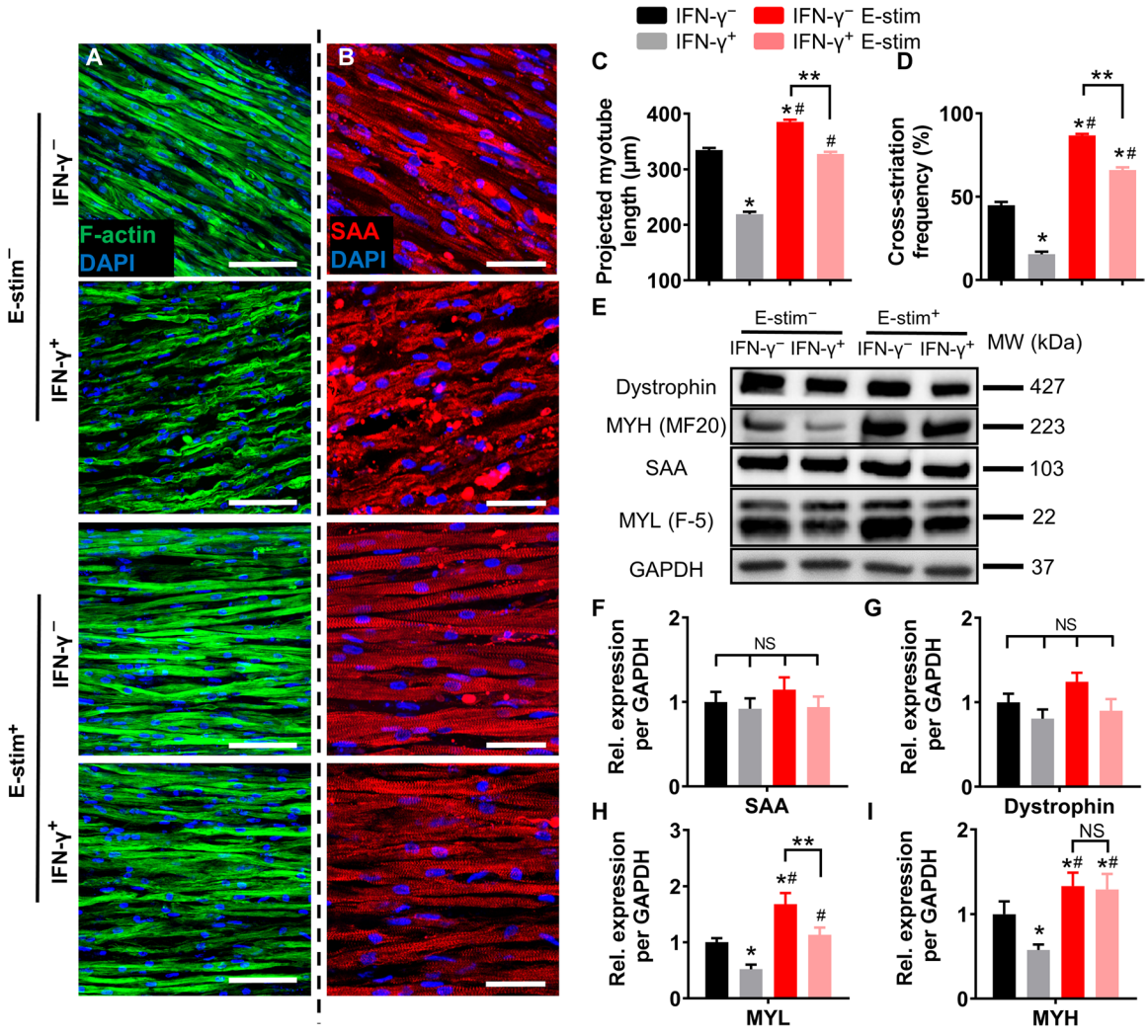

Fig. 3. E-stim prevents IFN-γ–induced decrease in myotube length, sarcomere abundance, and contractile protein expression. (**A** and **B**) Representative longitudinal myobundle sections immunostained for (A) F-actin (green; scale bars, 100 μm) and (B) SAA (red; scale bars, 50 μm). (**C** and **D**) Quantification of (C) projected myotube length ($n > 350$ myotubes from three donors per group) and (D) SAA cross-striation frequency ($n \geq 9$ images from each donor, $n \geq 37$ images per group). (**E**) Representative Western blots from a single donor showing expression of the sarcomeric proteins dystrophin, myosin heavy chain (MYH; MF20), SAA, and myosin light chain (MYL; F-5), with glyceraldehyde-3-phosphate dehydrogenase (GAPDH) serving as a loading control. (**F** to **I**) Quantification of Western blots averaged for three donors with protein abundance normalized to GAPDH and shown relative to IFN-γ^- group. *$P < 0.05$ versus IFN-γ^-, #$P < 0.05$ versus IFN-γ^+, **$P < 0.05$. NS, nonsignificant. Data are presented as means ± SEM.

as the changes in measured specific force (Fig. 3, E, H, and I). Specifically, MYL and MYH protein expressions were significantly reduced by IFN-γ treatment and were increased by E-stim in both untreated and, to a less extent, IFN-γ–treated myobundles. Regulation of MYL expression by skeletal muscle MYL kinase is associated with muscle differentiation (*34*) and the kinetics and amplitude of contractile force generation (*35*), while increase in MYH is associated with muscle differentiation, hypertrophy, and increased strength (*24*). Together, these studies showed that functional deficit due to IFN-γ treatment and benefit from E-stim could be at least in part explained by their opposite effects on contractile protein expression and organization.

E-stim prevents IFN-γ–induced deficit in myobundle calcium handling

To determine whether IFN-γ–induced force deficit may be additionally caused by impaired calcium handling, we measured myobundle Ca^{2+} transients using Fluo-8 AM dye (Fig. 4, A to D, and movie S2). IFN-γ treatment reduced calcium transient amplitude to ~60% of that in the untreated myobundles (Fig. 4E and table S1). E-stim caused a significant increase in Ca^{2+} transient amplitude in both untreated and IFN-γ–treated myobundles, consistent with changes in contractile force generation (Fig. 1G). To further obtain molecular insights in altered calcium handling in myobundles, we analyzed expression of RYR1 and CASQ1, proteins involved in sarcoplasmic reticulum Ca^{2+} release and buffering (Fig. 4F). Consistent with the observed decrease in Ca^{2+} transient amplitude, RYR1 and CASQ1 expressions were significantly reduced following IFN-γ treatment (Fig. 4, G and H). E-stim prevented the IFN-γ–induced effects, significantly increasing the expression of RYR1 and CASQ1 to and beyond the control levels in untreated myobundles (Fig. 4, G and H). Collectively, these results revealed that IFN-γ–induced weakness in myobundles was caused by deficits in both myotube structure and calcium handling.

E-stim partially prevents IFN-γ–induced changes in myobundle secretome

Regarding the known roles of IFN-γ in secretion and sensing of various cytokines, we quantified secretome of myobundles cultured in serum-free media in response to IFN-γ and/or E-stim using a multiplex bead–based assay (fig. S5). We found that application of IFN-γ increased myobundle secretion of several proinflammatory cytokines, namely, IL-7, IL-12p70, CX3CL1, IL-18, and monocyte chemoattractant protein-1 (MCP-1), and reduced myobundle secretion of IL-8 and leukemia inhibitory factor (LIF). E-stim altered myobundle secretome consistent with a report on human myotubes electrically stimulated short-term in serum-containing media (*36*). The cotreatment of myobundles with E-stim and IFN-γ partially or fully reversed the IFN-γ–induced effects on IL-12p70, IL-18, IL-8, and LIF and had no effects on MCP-1 or CX3CL1 secretion. Application of E-stim increased the myobundle secretion of IL-6 to a similar level with and without IFN-γ application, consistent with previous findings in mice suggesting that IFN-γ–induced muscle wasting is IL-6 independent (*9*).

E-stim attenuates up-regulation of JAK/STAT signaling induced by IFN-γ

Previous studies have suggested that proinflammatory effects of IFN-γ in muscle result from up-regulation of the JAK/STAT pathway (*37*). We thus measured the protein expression of total STAT1 and phosphorylated STAT1 (pSTAT1) and assessed the degree of STAT1 activation defined as pSTAT1/STAT1 (Fig. 4, I to L). We found that IFN-γ treatment increased both the total STAT1 and pSTAT1 levels as well as the ratio of pSTAT1/STAT1. While E-stim had no significant effects on STAT1 or pSTAT1 levels in the absence of IFN-γ, it significantly attenuated IFN-γ–induced pSTAT1 increase without affecting the levels of STAT1 (Fig. 4, I to L). Together, E-stim partially (~50%) attenuated the IFN-γ–induced up-regulation of the JAK/STAT1 pathway in myobundles, which, in addition to direct effects of E-stim on muscle hypertrophy and strengthening, represents a novel, independent mechanism for the beneficial anti-inflammatory effects of exercise on muscle weakness and wasting induced by IFN-γ.

JAK inhibitors prevent IFN-γ–induced deficits in myobundle force generation, structural organization, and protein expression

Beneficial effects of E-stim in conjunction with its partial down-regulation of JAK/STAT1 signaling prompted us to test in an independent set of experiments whether the direct inhibition of JAK/STAT pathway by Food and Drug Administration (FDA)–approved small-molecule inhibitors tofacitinib (Tofa, blocker of JAK1/2/3) and baricitinib (Bari, blocker of JAK1/2) can prevent structural and functional

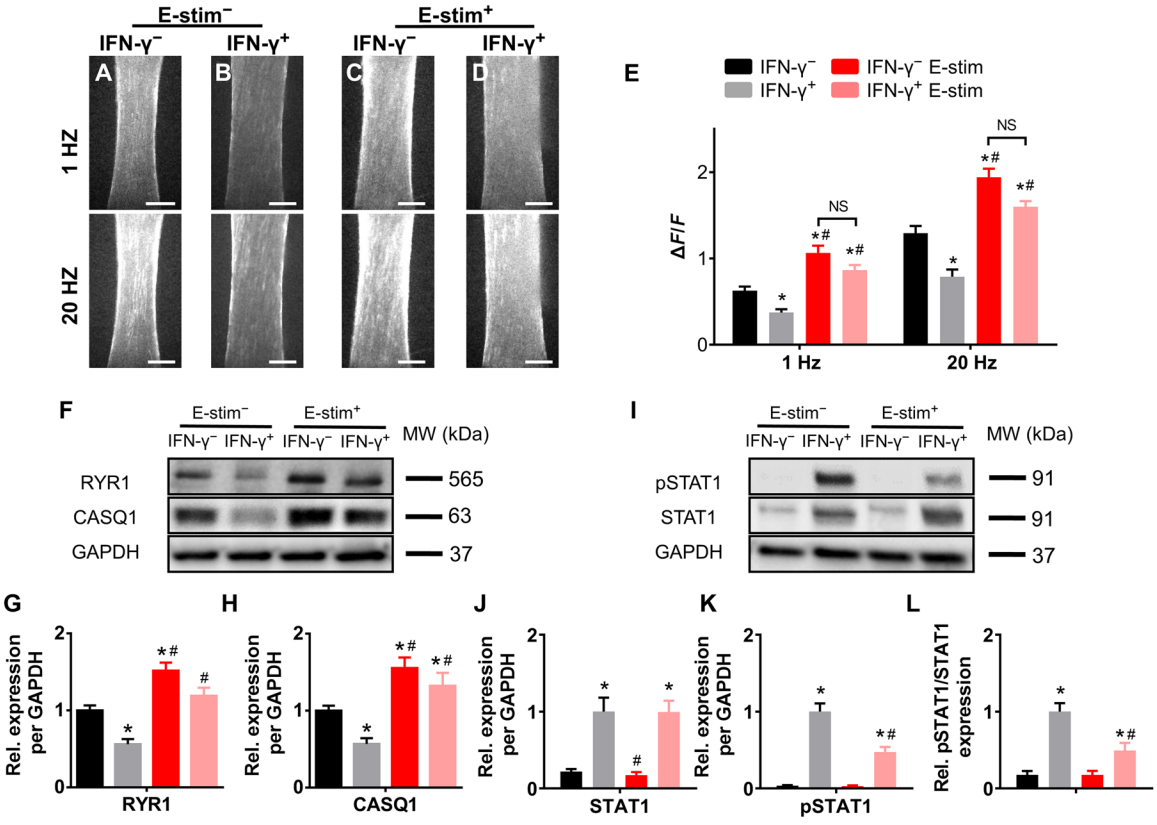

Fig. 4. E-stim counteracts IFN-γ–induced deficit in myobundle calcium handling and up-regulation of STAT1 signaling. (**A** to **D**) Representative peak Fluo-8 AM fluorescence intensity during E-stim (1 and 20 Hz) showing amplitudes of Ca^{2+} transients; scale bars, 500 μm. (**E**) Quantified amplitudes ($\Delta F/F$) of electrically stimulated Ca^{2+} transients based on Fluo-8 AM recording ($n = 8$ myobundles from one donor per group). (**F**) Representative Western blots for RYR1, CASQ1, and GAPDH (loading control). (**G** and **H**) Quantified (G) RYR1 and (H) CASQ1 protein expressions normalized to that of GAPDH and shown relative to IFN-γ^- group ($n = 6$ samples from three donors per group). (**I**) Representative Western blots for pSTAT1, STAT1, and GAPDH (loading control). (**J** to **L**) Quantified (J) STAT1, (K) pSTAT1, and (L) pSTAT1/STAT1 protein expressions normalized to that of GAPDH and shown relative to the IFN-γ^+ group ($n = 6$ samples from three donors per group). *$P < 0.05$ versus IFN-γ^-, #$P < 0.05$ versus IFN-γ^+. NS, nonsignificant. Data are presented as means ± SEM.

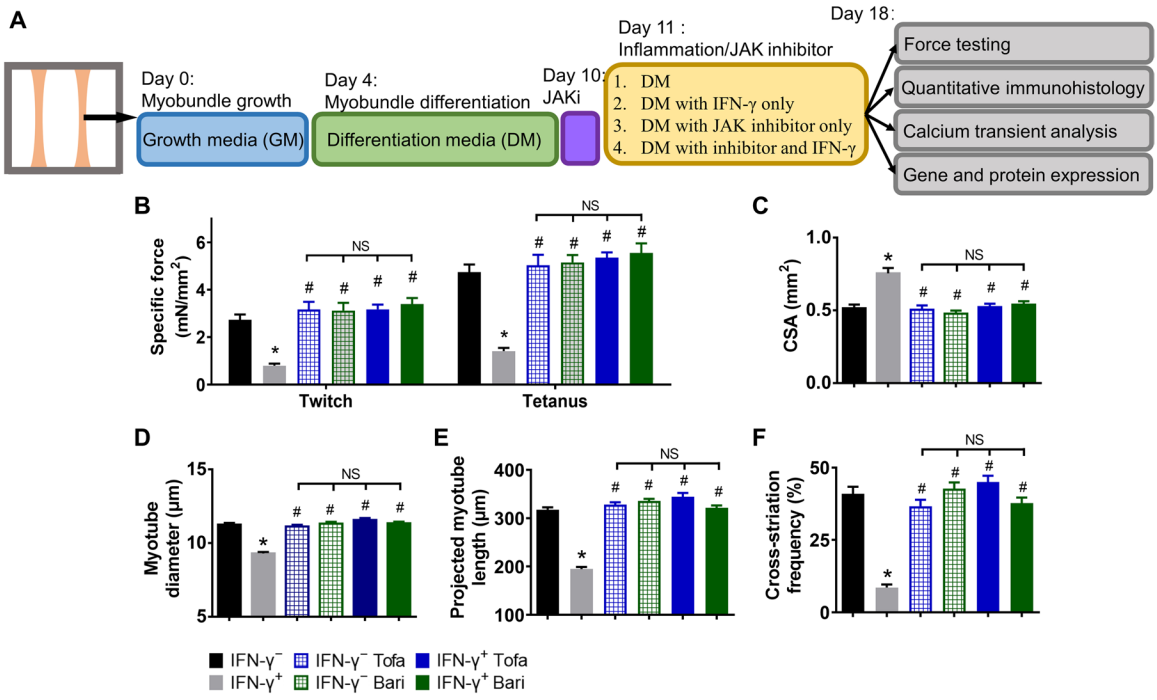

Fig. 5. JAK inhibitors prevent IFN-γ–induced deficits in myobundle force generation and structural organization. (**A**) Schematic overview of myobundle culture, treatment, and characterization. Human primary myoblasts were expanded in 2D culture and mixed with hydrogel to form 3D myobundles, which were cultured in GM for 4 days, then in DM for 6 days, after which JAK inhibitors (JAKi) tofacitinib (Tofa, 500 nM) or baricitinib (Bari, 500 nM) was applied for additional 8 days, the last 7 of which in the presence or absence of IFN-γ. (**B**) Contractile force amplitude per myobundle CSA (specific force, $n = 11$ to 15 myobundles from three donors per group). (**C**) Quantified CSA of myobundles. (**D**) Quantified myotube diameter from myobundle cross sections ($n \geq 720$ myotubes from three donors per group). (**E** and **F**) Quantified (E) projected myotube length ($n > 150$ myotubes from two donors per group) and (F) SAA cross-striation frequency ($n \geq 30$ images from three donors per group) from longitudinal sections of myobundles. *$P < 0.05$ versus IFN-γ$^-$, $^{\#}P < 0.05$ versus IFN-γ$^+$. NS, nonsignificant. Data are presented as means ± SEM.

deficits induced by IFN-γ (Fig. 5A). We found that 8-day treatment with either inhibitor (at a clinically relevant dose of 500 nM) had no adverse effects on myobundle morphology and function. On the other hand, the same dose of the inhibitors fully prevented the deteriorating effects of IFN-γ on myobundle contractile force and kinetics in all of the donors (Fig. 5B and fig. S6, A to F), as well as blocked the IFN-γ–induced increase in myobundle CSA (Fig. 5C) and decrease in myotube size, length, and abundance of cross-striations (Fig. 5, D to F, and fig. S7, A to C). The exact numerical results of functional measurements are presented in table S2. We next investigated whether JAK/STAT inhibitors prevented the IFN-γ–induced changes in myobundle contractile protein expression and calcium handling. Treatment of naïve myobundles with the inhibitors had no apparent effects on contractile or calcium handling protein expression or generation of Ca^{2+} transients (Fig. 6, A to F, and fig. S7, D and E). Coapplication of JAK/STAT inhibitors with IFN-γ fully prevented the IFN-γ–induced decrease in expression of MYL and MYH (Fig. 6, A to C), Ca^{2+} transient amplitude (Fig. 6D), and RYR1 and CASQ1 expression (Fig. 6, E and F), without any changes in dystrophin or SAA levels (fig. S7, D and E).

JAK inhibitors exert beneficial effect on IFN-γ–treated myobundles by preventing STAT1 activation

Because JAK/STAT inhibitors completely prevented the inflammatory action of IFN-γ on myobundles, we assessed their effects on STAT1 expression and activity by Western blotting. The treatment of naïve myobundles with tofacitinib did not affect the expression of STAT1 or pSTAT1, while baricitinib moderately increased the expression of STAT1 but not pSTAT1 (Fig. 6, G to I, and fig. S7F), consistent with previous studies (*38*). Application of the inhibitors to IFN-γ–treated myobundles significantly decreased pSTAT1 expression to near-naïve levels (Fig. 6, G and H), without altering the IFN-γ–induced increase in STAT1 expression (fig. S7F). Consequently, the IFN-γ–induced increase in STAT1 activity (pSTAT1/STAT1) was fully prevented by coapplication of the inhibitors, explaining their strong protective effects on myobundle function. Together, these results established that the adverse effect of IFN-γ on human myobundles was predominantly mediated via up-regulation of JAK/STAT1 signaling rather than changes in alternative signaling pathways (*39*).

DISCUSSION

Here, we used a human myobundle system to model inflammation-induced muscle weakness and explore anti-inflammatory mechanisms of muscle exercise. Previously, we have shown that myobundles represent a unique personalized in vitro platform to study not only structural and biochemical but also metabolic and contractile responses of human skeletal muscle to a diverse set of pathological and physiologic inputs, including exercise (*22*–*24*, *40*). In this study, we sought to explore how human skeletal muscle strength and structure are affected by IFN-γ, a prototypical cytokine elevated in various inflammatory diseases (*18*, *41*, *42*). Consistent with studies in mice (*13*, *14*), 7-day treatment of human myobundles with IFN-γ (20 ng/ml) induced muscle weakness (i.e., weaker and slower contractions) that

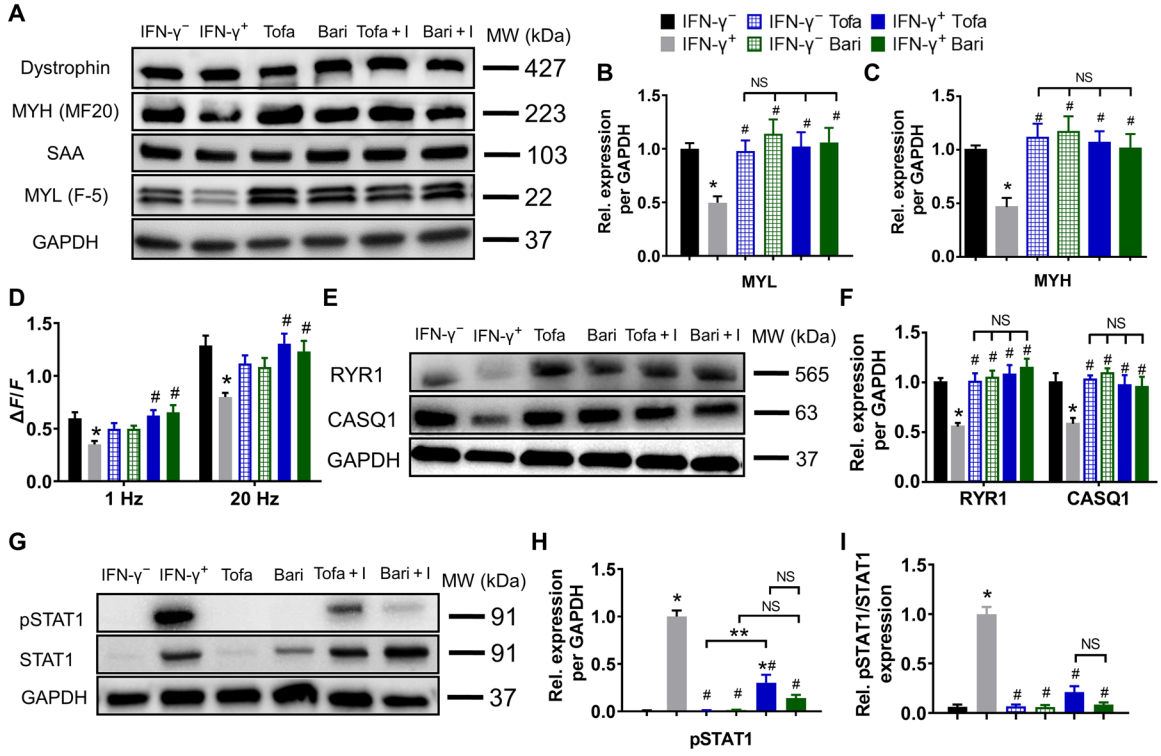

Fig. 6. JAK inhibitors prevent IFN-γ–induced protein down-regulation and STAT1 activation in myobundles. (**A**) Representative Western blots from a single donor showing expression of dystrophin, MYH (MF20), SAA, and MYL (F-5), with GAPDH serving as a protein loading control. Tofa + I: tofacitinib + IFN-γ, Bari + I: baricitinib + IFN-γ. (**B** and **C**) Quantifications of Western blots for (B) MYL and (C) MYH averaged for three donors with protein abundance normalized to GAPDH and shown relative to IFN-γ^- group ($n = 6$ samples from three donors per group). No difference in dystrophin or SAA expression was observed. (**D**) Quantified amplitudes of electrically stimulated (1 and 20 Hz) Ca^{2+} transients ($n = 8$ myobundles from one donor per group). (**E**) Representative Western blots for RYR1, CASQ1, and GAPDH. (**F**) Quantified RYR1 and CASQ1 protein expression normalized to that of GAPDH and shown relative to the IFN-γ^- group ($n = 6$ samples from three donors per group). (**G**) Representative Western blots for pSTAT1, STAT1, and GAPDH. (**H** and **I**) Quantified (H) pSTAT1 and (I) pSTAT1/STAT1 protein expression normalized to that of GAPDH and shown relative to the IFN-γ^+ group ($n = 3$ samples from three donors per group). *$P < 0.05$ versus IFN-γ^-, #$P < 0.05$ versus IFN-γ^+; **$P < 0.05$. NS, nonsignificant. Data are presented as means ± SEM.

was associated with significant myofiber atrophy and disarray, reduced expression of contractile and calcium handling proteins, and altered cytokine expression. These results were fully reproduced in myobundles derived from three independent donors. When coapplied with IFN-γ, a 7-day intermittent exercise-mimetic E-stim had pronounced protective effects on myobundles. Beside its well-established hypertrophic and strengthening effects (*24*, *43*), the exercise-mimetic E-stim (*24*) partially reduced IFN-γ–induced STAT1 up-regulation, established using selective JAK/STAT inhibitors to be the dominant proinflammatory mediator of IFN-γ action in myobundles. To our knowledge, this is the first study to explore direct and specific effects of IFN-γ on human skeletal muscle function and to demonstrate the existence of a novel myofiber-autonomous, anti-inflammatory mechanism of muscle exercise involving the JAK/STAT1 pathway (fig. S8). We anticipate the future use of myobundle platform to study human inflammatory disease and anti-inflammatory therapies.

Skeletal muscle is an important secretory organ in the body that both responds to systemic endocrine signals and can function as an active regulator of immune and inflammatory response. Physical exercise can alter the cytokine secretion of skeletal muscle and other tissues, which in turn can promote muscle repair after injury (*44*), inhibit muscle atrophy (*26*), and potentially act as an anti-inflammatory therapy in chronic inflammatory diseases (*27*). While the anti-inflammatory effect of exercising muscle fibers has been mainly attributed to their paracrine cross-talk with proinflammatory non-muscle cells (*29*), the use of myobundles devoid of immune or fat cells in this study allowed us to unveil muscle-autonomous inhibitory effects of exercise on JAK/STAT1 signaling, a mediator of muscle inflammation caused by IFN-γ. This exercise-induced down-regulation of pSTAT1 could be autocrine mediated via the partial normalization of IFN-γ–induced changes in myobundle secretome; however, pleotropic effects of muscle exercise on several intracellular signaling pathways (*45*) and their potential cross-talk with JAK/STAT signaling (*39*, *46*, *47*) warrant future investigations. Our studies also confirmed that the FDA-approved small-molecule JAK/STAT inhibitors tofacitinib and baricitinib, prescribed for rheumatoid arthritis, fully prevented IFN-γ–induced muscle wasting at a non-toxic, therapeutically relevant dose (*32*), although their biochemical mechanisms of action may vary based on the somewhat differing effects on STAT1 and pSTAT1 expression.

In summary, we have applied an in vitro 3D myobundle model to investigate the interplay between IFN-γ and exercise-mimetic stimulation in inflammatory response of human skeletal muscle. We show that chronic application of IFN-γ induces myobundle weakness via up-regulation of JAK/STAT1 signaling pathway, which can be partially prevented by exercise-mimetic stimulation and fully prevented by treatment with clinically approved JAK/STAT inhibitors.

We envision that incorporation of additional human nonmuscle cells in the myobundle platform [akin to use of macrophages in a rat skeletal muscle model (*40*)] multiplexed with application of various inflammatory cytokines (*18*), exercise-mimetic regimes (*24*), and candidate therapeutics will allow comprehensive mechanistic studies of human muscle inflammation, anti-inflammatory roles of exercise, and discovery of effective therapies for muscle wasting.

MATERIALS AND METHODS

Isolation of human myoblasts

Human skeletal muscle samples were obtained from three donors (two females and one male, age 12 to 18) through standard needle biopsy or surgical waste from three donors with informed consent under Duke University Institutional Review Board–approved protocols (Pro00048509 and Pro00012628). Muscle tissue was minced using sharp scissors and enzymatically digested with 0.05% trypsin for 30 min at 37°C. Isolated cells were collected by centrifugation and resuspended in growth media [GM; low-glucose Dulbecco's modified Eagle's medium (DMEM) (Thermo Fisher Scientific, D6046) supplemented with 10% fetal bovine serum (FBS) (Hyclone, SH30071.03), fetuin (50 μg/ml) from FBS (Sigma-Aldrich, F2379), recombinant human epidermal growth factor (EGF) (PeproTech, AF-100-15), dexamethasone (Sigma-Aldrich, F2379), and penicillin G (100 U/ml, Thermo Fisher Scientific)] and preplated for 2 hours to reduce the number of fibroblasts. After preplating, the cells were transferred onto to 1% Matrigel (BD Biosciences)–coated flasks, cultured in GM, and expanded by passaging after reaching 70% confluence. At passage 4 or 5, cells were detached, counted, and used to fabricate myobundles.

Formation and culture of engineered human myobundles

Human myobundles were fabricated as described previously (*23*, *24*). Briefly, polydimethylsiloxane (PDMS) molds made to fit in a well of a 12-well plate were casted from 3D-machined Teflon masters containing two semicylindrical wells (7 mm long, 2-mm diameter for culture of two myobundles), sterilized in 70% ethanol, air dried in a tissue culture hood, and coated with 0.2% (w/v) Pluronic F-127 (Invitrogen) for at least 1 hour at room temperature to prevent tissue adhesion. Laser-cut Cerex frames (9×9 mm^2, 1-mm-wide rim) were sterilized and placed within the air-dried PDMS molds. The frame provided an anchor surface for myobundle attachment and functioned as a mechanical guide during cell-mediated hydrogel compaction, resulting in uniaxial cell alignment (*48*). Expanded myogenic cells were dissociated using 0.025% trypsin-EDTA and encapsulated in a hydrogel solution at 1.5×10^7 cells/ml. For a single myobundle, the cell/hydrogel solution contained 10 μl of bovine fibrinogen (20 mg/ml) in phosphate-buffered saline (PBS) (Sigma-Aldrich), 10 μl of Matrigel (Corning), 2 μl of bovine thrombin (50 U/ml) in 0.1% bovine serum albumin (BSA) in PBS (Sigma-Aldrich), and 28.2 μl of GM with 0.75×10^6 cells, prepared on ice, which was mixed thoroughly and immediately pipetted into one well of the PDMS mold. Cell/hydrogel mixture in PDMS molds was polymerized at 37°C for 30 min, and thereafter, myobundles were cultured on a rocker. After 2 days, frames with myobundles were removed from the molds and left to float in culture media. GM was used for the first 4 days of culture, after which it was replaced by differentiation medium [DM, low glucose DMEM (Thermo Fisher Scientific) supplemented with N2 supplement (100×, Thermo Fisher Scientific), penicillin G (100 U/ml, Thermo Fisher Scientific)], with media changes performed daily. Media were supplemented with 6-aminocaproic acid (ACA; Sigma-Aldrich) to reduce fibrinolysis (1.5 mg/ml in GM. 2 mg/ml in DM).

E-stim and pharmacological treatment of myobundles

For inflammation experiments, starting on differentiation day 7 (culture day 11), myobundles were treated for an additional 7 days with IFN-γ (20 ng/ml) [PeproTech, 300-02, in BSA final (0.5 μg/ml)] freshly added during each media change. Control group was supplemented with media only. For E-stim experiments, we used custom-made PDMS chambers containing two parallel carbon electrodes, as previously described (*24*, *49*). Myobundles were placed in the chamber, and E-stim was applied from differentiation days 7 to 14 either without or with IFN-γ treatment using a D330 MultiStim system (Digitimer Ltd.) controlled by a custom-made LabVIEW program. The applied intermittent regime of stimulation consisted of 1-hour stimulation cycles (bipolar 2 ms, 70-mA constant-current impulses applied in 0.5-s-long 10-Hz pulse trains delivered every 5 s) separated by 7-hour rests (Fig. 1B) (*24*). For experiments with JAK/STAT inhibitors, tofacitinib (in water; Sigma-Aldrich, PZ0017) or baricitinib (in 0.01% DMSO final; Sigma-Aldrich, G-5743,) was added at 500 nM concentration to myobundles starting on differentiation day 6, 1 day before IFN-γ treatment, and continued to be freshly applied (with or without IFN-γ) for the following 8 days during the daily media changes.

Isometric measurements of contractile force generation

Contractile force generation and passive tension in myobundles were measured using a previously described custom-made force measurement apparatus (*22*). Briefly, single myobundles were transferred to the force measurement apparatus and immersed in DMEM media at 37°C. One end of the myobundle was attached to a fixed PDMS block, and the other to a movable PDMS float connected to a force transducer mounted on a computer-controlled motorized linear actuator (Thorlabs, Newton, NJ). The sides of the frame were cut to allow force measurements. Using the linear actuator, the myobundle was stretched to 100, 108, and 116% of their original culture length, and twitch contractions were recorded in response to 10-ms electrical pulses applied by platinum electrodes at 1-Hz stimulation rate. At 16% stretch, 1-s-long stimulation at 20 Hz was applied to record tetanic contractile force. Force traces were analyzed for peak twitch and tetanus force, passive tension, time-to-peak twitch, and half-relaxation time using a custom MATLAB program (*22*, *40*).

Immunohistology

Myobundles were fixed in 2% (v/v) paraformaldehyde (Electron Microscopy Sciences) in PBS overnight at 4°C with rocking. Fixed samples were submerged in optimal cutting temperature compound (Electron Microscopy Sciences) and snap frozen in liquid nitrogen. Constructs were sectioned (10 μm thick) parallel (longitudinal) and perpendicular (cross) to the long axis of the bundles using a cryostat (LEICA CM1950) and were mounted onto glass slides. Before staining, sections were incubated in a blocking solution containing 5% chick serum and 0.1% Triton X-100 in PBS overnight at 4°C. Primary antibodies were applied in blocking solution overnight at 4°C. Secondary antibodies were applied overnight at 4°C. Antibody information and dilutions are listed in table S3. Immunostained samples were mounted with ProLong Glass

Antifade reagent (Thermo Fisher Scientific, P36984). Fluorescence images were acquired using an Andor Dragonfly spinning disk confocal microscope at ×10 to ×40 magnification and analyzed by ImageJ.

Analysis of myotube organization

Images of myobundle longitudinal sections stained for F-actin and SAA were used for the measurement of myotube organization. Projected length of clearly distinguishable F-actin–labeled myotubes was determined manually (fig. S3, A and B). Percentage of cross-striated myotubes was assessed by manually counting the cross-striated myotubes labeled by SAA staining divided by the total number of myotubes determined from F-actin costaining of the same section.

Quantitative cytokine expression analysis

Media conditioned by myobundles from three donors were collected between days 3 and 4 of E-stim for the E-stim groups and on equivalent culture days (between days 14 and 15) for the groups without E-stim, then frozen, and used for the secretome analysis on the same plate upon thawing. Select cytokine concentrations were measured using a custom-designed human magnetic 18-plex panel for the Luminex platform (Thermo Fisher Scientific, Waltham, MA) by the Immunology Core at Duke University following the manufacturer's instructions.

Western blotting

Protein was isolated from three to four myobundles per experimental sample in ice-cold radioimmunoprecipitation assay lysis and extraction buffer in the presence of protease inhibitor (Sigma-Aldrich) and phosphatase inhibitor cocktail (Roche), as previously described (*24*). Protein concentration was determined using a bicinchoninic acid assay (Thermo Fisher Scientific). Western blots were performed using Bio-Rad Mini-PROTEAN 4 to 15% gradient gels with proteins transferred using a Bio-Rad Mini Trans-Blot Cell. After blocking with 5% milk or 5% BSA in tris-buffered saline with 0.1% Tween 20 at room temperature for 1 hour, primary antibodies diluted in the same blocking solution were incubated with the membrane at 4°C overnight. Horseradish peroxidase–conjugated anti-mouse and anti-rabbit secondary antibodies were applied for 1 hour at room temperature. Antibody information and dilutions are listed in table S3. Protein detection was performed using either SuperSignal West Pico PLUS or Femto Maximum ECL chemiluminescence substrates (Thermo Fisher Scientific). Images were acquired using a Bio-Rad ChemiDoc imaging system and analyzed with ImageJ.

Measurements of calcium transients

For Ca^{2+} transient measurements, myobundles were incubated with 50 μM of calcium-sensitive dye Fluo-8 AM (Abcam, ab142773) in DM in an incubator for 1 hour while rocking, followed by washing in dye-free media for 30 min. Electrically induced Ca^{2+} transients were recorded as previously described (*24*, *40*). Myobundles were transferred into a glass-bottom live-imaging chamber with Tyrode's solution warmed at 37°C in a heated live-imaging chamber. Fluorescence images were acquired at ×4 magnification on a Nikon microscope using a high speed EMCCD (electron multiplying charge-coupled device) camera (Andor iXon 860) and Andor Solis software. Ca^{2+} transient amplitudes were calculated as the maximum relative change in fluorescence signal, $\Delta F/F$ = (Peak − Trough)/(Trough − Background).

Statistical analysis

Experimental data are presented as means ± SEM. Statistical significances between groups were verified by one-way analysis of variance (ANOVA) with Tukey's post hoc test or as described in the figure captions, using GraphPad Prism (GraphPad Software). $P < 0.05$ was considered statistically significant. Sample sizes for in vitro experiments were determined based on variance of previously reported measurements. All immunostaining images and movies shown are representative of similar results from at least three independent experiments.

SUPPLEMENTARY MATERIALS

Supplementary material for this article is available at http://advances.sciencemag.org/cgi/content/full/7/4/eabd9502/DC1

View/request a protocol for this paper from *Bio-protocol*.

REFERENCES AND NOTES

1. J. G. Tidball, Inflammatory processes in muscle injury and repair. *American Journal of Physiology-Regulatory, Integrative and Comparative Physiology* **288**, R345–R353 (2005).
2. M. Panduro, C. Benoist, D. Mathis, T(reg) cells limit IFN-γ production to control macrophage accrual and phenotype during skeletal muscle regeneration. *Proc. Natl. Acad. Sci. U.S.A.* **115**, E2585–E2593 (2018).
3. D. D. Sin, S. F. Man, Skeletal muscle weakness, reduced exercise tolerance, and COPD: Is systemic inflammation the missing link? *Thorax* **61**, 1–3 (2006).
4. J. Walsmith, R. Roubenoff, Cachexia in rheumatoid arthritis. *Int. J. Cardiol.* **85**, 89–99 (2002).
5. M. Salajegheh, S. W. Kong, J. L. Pinkus, R. J. Walsh, A. Liao, R. Nazareno, A. A. Amato, B. Krastins, C. Morehouse, B. W. Higgs, B. Jallal, Y. Yao, D. A. Sarracino, K. C. Parker, S. A. Greenberg, Interferon-stimulated gene 15 (ISG15) conjugates proteins in dermatomyositis muscle with perifascicular atrophy. *Ann. Neurol.* **67**, 53–63 (2010).
6. W. J. Evans, Skeletal muscle loss: Cachexia, sarcopenia, and inactivity. *Am. J. Clin. Nutr.* **91**, 1123S–1127S (2010).
7. D. Califano, Y. Furuya, S. Roberts, D. Avram, A. N. J. McKenzie, D. W. Metzger, IFN-γ increases susceptibility to influenza A infection through suppression of group II innate lymphoid cells. *Mucosal Immunol.* **11**, 209–219 (2018).
8. N. Chen, M. Zhou, X. Dong, J. Qu, F. Gong, Y. Han, Y. Qiu, J. Wang, Y. Liu, Y. Wei, J. Xia, T. Yu, X. Zhang, L. Zhang, Epidemiological and clinical characteristics of 99 cases of 2019 novel coronavirus pneumonia in Wuhan, China: A descriptive study. *Lancet* **395**, 507–513 (2020).
9. J. F. Ma, B. J. Sanchez, D. T. Hall, A. K. Tremblay, S. Di Marco, I. E. Gallouzi, STAT3 promotes IFNγ/TNFα-induced muscle wasting in an NF-κB-dependent and IL-6-independent manner. *EMBO Mol. Med.* **9**, 622–637 (2017).
10. T. F. Gajewski, F. W. Fitch, Anti-proliferative effect of IFN-gamma in immune regulation. I. IFN-gamma inhibits the proliferation of Th2 but not Th1 murine helper T lymphocyte clones. *The Journal of Immunology* **140**, 4245–4252 (1988).
11. G. D. Shelton, N. A. Calcutt, R. S. Garrett, D. Gu, N. Sarvetnick, W. M. Campana, H. C. Powell, Necrotizing myopathy induced by overexpression of interferon-gamma in transgenic mice. *Muscle Nerve* **22**, 156–165 (1999).
12. R. L. Reinhardt, H.-E. Liang, K. Bao, A. E. Price, M. Mohrs, B. L. Kelly, R. M. Locksley, A novel model for IFN-γ–mediated autoinflammatory syndromes. *The Journal of Immunology* **194**, 2358–2368 (2015).
13. S. A. Villalta, B. Deng, C. Rinaldi, M. Wehling-Henricks, J. G. Tidball, IFN-γ promotes muscle damage in the mdx mouse model of Duchenne muscular dystrophy by suppressing M2 macrophage activation and inhibiting muscle cell proliferation. *The Journal of Immunology* **187**, 5419–5428 (2011).
14. P. Londhe, J. K. Davie, Gamma interferon modulates myogenesis through the major histocompatibility complex class II transactivator, CIITA. *Mol. Cell. Biol.* **31**, 2854–2866 (2011).
15. P. Londhe, D. C. Guttridge, Inflammation induced loss of skeletal muscle. *Bone* **80**, 131–142 (2015).
16. R. Hohlfeld, A. G. Engel, Induction of HLA-DR expression on human myoblasts with interferon-gamma. *Am. J. Pathol.* **136**, 503–508 (1990).
17. E. Gallardo, I. de Andrés, I. Illa, Cathepsins are upregulated by IFN-gamma/STAT1 in human muscle culture: A possible active factor in dermatomyositis. *J. Neuropathol. Exp. Neurol.* **60**, 847–855 (2001).
18. K. Nagaraju, N. Raben, G. Merritt, L. Loeffler, K. Kirk, P. Plotz, A variety of cytokines and immunologically relevant surface molecules are expressed by normal human skeletal muscle cells under proinflammatory stimuli. *Clin. Exp. Immunol.* **113**, 407–414 (1998).

19. R. Raju, O. Vasconcelos, R. Granger, M. C. Dalakas, Expression of IFN-gamma-inducible chemokines in inclusion body myositis. *J. Neuroimmunol.* **141**, 125–131 (2003).
20. A. E. Kalovidouris, Z. Plotkin, D. Graesser, Interferon-gamma inhibits proliferation, differentiation, and creatine kinase activity of cultured human muscle cells. II. A possible role in myositis. *J Rheumatol* **20**, 1718–1723 (1993).
21. J. Wang, A. Khodabukus, L. Rao, K. Vandusen, N. Abutaleb, N. Bursac, Engineered skeletal muscles for disease modeling and drug discovery. *Biomaterials* **221**, 119416 (2019).
22. L. Madden, M. Juhas, W. E. Kraus, G. A. Truskey, N. Bursac, Bioengineered human myobundles mimic clinical responses of skeletal muscle to drugs. *eLife* **4**, e04885 (2015).
23. L. Rao, Y. Qian, A. Khodabukus, T. Ribar, N. Bursac, Engineering human pluripotent stem cells into a functional skeletal muscle tissue. *Nat. Commun.* **9**, 126 (2018).
24. A. Khodabukus, L. Madden, N. K. Prabhu, T. R. Koves, C. P. Jackman, D. M. Muoio, N. Bursac, Electrical stimulation increases hypertrophy and metabolic flux in tissue-engineered human skeletal muscle. *Biomaterials* **198**, 259–269 (2019).
25. M. F. Ahmad, A. H. Hasbullah, The effects of electrical muscle stimulation (EMS) towards male skeletal muscle mass. *Int J Sport Health Sci* **9**, 864–873 (2015).
26. R. Roubenoff, Physical activity, inflammation, and muscle loss. *Nutr. Rev.* **65**, S208–S212 (2007).
27. M. Gleeson, N. C. Bishop, D. J. Stensel, M. R. Lindley, S. S. Mastana, M. A. Nimmo, The anti-inflammatory effects of exercise: Mechanisms and implications for the prevention and treatment of disease. *Nat. Rev. Immunol.* **11**, 607–615 (2011).
28. A. Karlsen, C. K. Cullum, K. L. Norheim, F. U. Scheel, A. H. Zinglersen, J. Vahlgren, P. Schjerling, M. Kjaer, A. L. Mackey, Neuromuscular Electrical Stimulation Preserves Leg Lean Mass in Geriatric Patients. *Med. Sci. Sports Exerc.* **52**, 773–784 (2020).
29. S. Schnyder, C. Handschin, Skeletal muscle as an endocrine organ: PGC-1α, myokines and exercise. *Bone* **80**, 115–125 (2015).
30. S. Pérez-Baos, I. Prieto-Potin, J. A. Román-Blas, O. Sánchez-Pernaute, R. Largo, G. Herrero-Beaumont, Mediators and patterns of muscle loss in chronic systemic inflammation. *Front. Physiol.* **9**, 409 (2018).
31. W. J. Sandborn, S. Ghosh, J. Panes, I. Vranic, C. Su, S. Rousell, W. Niezychowski, Tofacitinib, an oral Janus kinase inhibitor, in active ulcerative colitis. *New England Journal of Medicine* **367**, 616–624 (2012).
32. J. G. Shi, X. Chen, F. Lee, T. Emm, P. A. Scherle, Y. Lo, N. Punwani, W. V. Williams, S. Yeleswaram, The pharmacokinetics, pharmacodynamics, and safety of baricitinib, an oral JAK 1/2 inhibitor, in healthy volunteers. *The Journal of Clinical Pharmacology* **54**, 1354–1361 (2014).
33. F. Cantini, L. Niccoli, D. Matarrese, E. Nicastri, P. Stobbione, D. Goletti, Baricitinib therapy in COVID-19: A pilot study on safety and clinical impact. *J. Infect.* **81**, 318–356 (2020).
34. G. Zhi, J. W. Ryder, J. Huang, P. Ding, Y. Chen, Y. Zhao, K. E. Kamm, J. T. Stull, Myosin light chain kinase and myosin phosphorylation effect frequency-dependent potentiation of skeletal muscle contraction. *Proc. Natl. Acad. Sci.* **102**, 17519–17524 (2005).
35. J. W. Ryder, K. S. Lau, K. E. Kamm, J. T. Stull, Enhanced skeletal muscle contraction with myosin light chain phosphorylation by a calmodulin-sensing kinase. *J. Biol. Chem.* **282**, 20447–20454 (2007).
36. M. Scheler, M. Irmler, S. Lehr, S. Hartwig, H. Staiger, H. Al-Hasani, J. Beckers, M. H. de Angelis, H. U. Häring, C. Weigert, Cytokine response of primary human myotubes in an in vitro exercise model. *Am. J. Physiol. Cell Physiol.* **305**, C877–C886 (2013).
37. L. Sun, K. Ma, H. Wang, F. Xiao, Y. Gao, W. Zhang, K. Wang, X. Gao, N. Ip, Z. Wu, JAK1–STAT1–STAT3, a key pathway promoting proliferation and preventing premature differentiation of myoblasts. *J. Cell Biol.* **179**, 129–138 (2007).
38. C. Liu, R. Arnold, G. Henriques, K. Djabali, Inhibition of JAK-STAT Signaling with Baricitinib Reduces Inflammation and Improves Cellular Homeostasis in Progeria Cells. *Cell* **8**, 1276 (2019).
39. D. J. Gough, D. E. Levy, R. W. Johnstone, C. J. Clarke, IFNgamma signaling-does it mean JAK-STAT? *Cytokine Growth Factor Rev.* **19**, 383–394 (2008).
40. M. Juhas, N. Abutaleb, J. T. Wang, J. Ye, Z. Shaikh, C. Sriworarat, Y. Qian, N. Bursac, Incorporation of macrophages into engineered skeletal muscle enables enhanced muscle regeneration. *Nature biomedical engineering* **2**, 942–954 (2018).
41. K. M. Pollard, D. M. Cauvi, C. B. Toomey, K. V. Morris, D. H. Kono, Interferon-γ and systemic autoimmunity. *Discov. Med.* **16**, 123–131 (2013).
42. X. Hu, L. B. Ivashkiv, Cross-regulation of signaling pathways by interferon-gamma: Implications for immune responses and autoimmune diseases. *Immunity* **31**, 539–550 (2009).
43. G. B. Stene, J. L. Helbostad, T. R. Balstad, I. I. Riphagen, S. Kaasa, L. M. Oldervoll, Effect of physical exercise on muscle mass and strength in cancer patients during treatment--a systematic review. *Crit. Rev. Oncol. Hematol.* **88**, 573–593 (2013).
44. K. M. Khan, A. Scott, Mechanotherapy: How physical therapists' prescription of exercise promotes tissue repair. *Br. J. Sports Med.* **43**, 247–252 (2009).
45. L. A. Perandini, P. Chimin, D. D. S. Lutkemeyer, N. O. S. Câmara, Chronic inflammation in skeletal muscle impairs satellite cells function during regeneration: Can physical exercise restore the satellite cell niche? *FEBS J.* **285**, 1973–1984 (2018).
46. N. Li, J. E. McLaren, D. R. Michael, M. Clement, C. A. Fielding, D. P. Ramji, ERK is integral to the IFN-γ-mediated activation of STAT1, the expression of key genes implicated in atherosclerosis, and the uptake of modified lipoproteins by human macrophages. *J. Immunol.* **185**, 3041–3048 (2010).
47. C. He, H. Li, B. Viollet, M. H. Zou, Z. Xie, AMPK Suppresses Vascular Inflammation In Vivo by Inhibiting Signal Transducer and Activator of Transcription-1. *Diabetes* **64**, 4285–4297 (2015).
48. S. Hinds, W. Bian, R. G. Dennis, N. Bursac, The role of extracellular matrix composition in structure and function of bioengineered skeletal muscle. *Biomaterials* **32**, 3575–3583 (2011).
49. C. Jackman, H. Li, N. Bursac, Long-term contractile activity and thyroid hormone supplementation produce engineered rat myocardium with adult-like structure and function. *Acta Biomater.* **78**, 98–110 (2018).

Acknowledgments: We thank A. Khodabukus for technical advice and K. Huang for advice on writing the manuscript. **Funding:** Research reported in this study was supported by the NIH under grants UH3TR002142, U01EB028901, and R01AR070543. The content of the manuscript is solely the responsibility of the authors and does not necessarily represent the official views of the NIH. **Author contributions:** N.B., L.R., and Z.C. conceived the idea and designed the experiments; Z.C., L.R., B.L., and R.-Z.Z. performed the experiments and analyzed the data; Z.C. and N.B. wrote the manuscript. **Competing interests:** The authors declare that they have no competing interests. **Data and materials availability:** All data needed to evaluate the conclusions in the paper are present in the paper and/or the Supplementary Materials. Additional data related to this paper may be requested from the authors.

Submitted 24 July 2020
Accepted 3 December 2020
Published 22 January 2021
10.1126/sciadv.abd9502

Citation: Z. Chen, B. Li, R.-Z. Zhan, L. Rao, N. Bursac, Exercise mimetics and JAK inhibition attenuate IFN-γ–induced wasting in engineered human skeletal muscle. *Sci. Adv.* **7**, eabd9502 (2021).